Article

Composite Switched Lyapunov Function-Based Control of DC–DC Converters for Renewable Energy Applications

Tohid Hashemi [1], Reza Mahboobi Esfanjani [2] and Hamed Jafari Kaleybar [1,*]

1   Energy Department, Politecnico di Milano, 20156 Milan, Italy; tohid.hashemi@mail.polimi.it
2   Electrical Engineering Department, Sahand University of Technology, Tabriz 51335-1996, Iran; mahboobi@sut.ac.ir
*   Correspondence: hamed.jafari@polimi.it

Abstract: Renewable energy sources play a pivotal role in the pursuit of sustainable and eco-friendly power solutions. While offering environmental benefits, they present inherent challenges. Photovoltaic systems rely on surrounding conditions, wind systems contend with variable wind speeds, and fuel cells are both costly and inefficient. Furthermore, the energy injected by renewable energy sources (RES) exhibits unpredictable behavior. To tackle these problems, researchers employ diverse power electronic devices and converters like inverters, power quality filters, and DC–DC choppers. Among these, DC–DC converters stand out for effectively regulating DC voltage and enhancing the efficiency of RESs. The meticulous selection of a suitable DC–DC converter, coupled with the integration of an efficient control technique, significantly influences overall power system performance. This paper introduces a novel approach to the design of switching controllers for DC–DC converters, specifically tailored for application in renewable energy systems. The proposed controller leverages the power of composite switched Lyapunov functions (CSLF) to enhance the efficiency and performance of DC–DC converters, addressing the unique challenges posed by renewable energy sources. Through comprehensive analysis and simulation, this study demonstrates the efficacy of the controller in optimizing power transfer, improving stability, and ensuring reliable operation in diverse renewable energy environments. Moreover, the small-scale DC–DC converter experiment's findings are presented to confirm and validate the proposed scheme's practical applicability.

Keywords: switched systems; DC–DC converters; renewable energy sources; composite Lyapunov functions; guaranteed cost control

1. Introduction

In recent decades, there has been a notable surge of interest in step-up DC–DC converters across diverse applications, particularly in renewable energy sources such as photovoltaic (PV) and fuel cell (FC). These interface circuits convert low-input voltage (below 50 V) into a controlled and elevated output voltage [1]. The innovation of pulse-width modulated (PWM) boost converters has led to the evolution of switched-mode step-up DC–DC converters. These configurations elevate output voltage by temporarily storing and releasing energy from the input, utilizing magnetic field storage components (e.g., inductors) or electric field storage components (e.g., capacitors) with active or passive switching elements [2].

DC–DC converters are playing a pivotal role in enhancing the efficiency and viability of smart grids and microgrids, especially in the context of integrating renewable energy sources. Meanwhile, in the electric transportation sector, the application of DC–DC converters is instrumental in addressing the diverse voltage requirements of components within electric vehicles (EVs) [3] or their integration with electric railway systems [4]. Various sources, such as batteries and supercapacitors, often produce output voltages that may fall below the levels needed for efficient power conversion. Elevating these voltages becomes

crucial to meet the demands of electric propulsion systems and other vehicle subsystems. High step-up DC/DC converters are essential in this context, serving as key components to ensure optimal energy conversion, distribution, and utilization in EVs. Overcoming the limitations associated with conventional converters is vital for enhancing overall efficiency, extending the range of electric vehicles, and promoting the broader adoption of sustainable transportation solutions. In Figure 1, an illustration of an integrated hybrid renewable energy grid-connected system linked with a sustainable transportation system [5] is depicted, where various sources, such as photovoltaic arrays, fuel stacks, supercapacitors, or batteries as energy storage systems (ESS), generated relatively low-output voltages, often below 48 V. To seamlessly integrate these sources into an AC grid-connected power system, or even a DC charging station, a crucial step involved boosting the generated low voltages to higher levels, like 380–760 V for a full-bridge and a half-bridge inverter. Furthermore, integrating two DC hub-like local DC bus and metro or tramway DC lines, as shown in Figure 1, can be realized by such DC–DC converters [6]. Accordingly, the realization of step-up DC/DC converters with superior performance has stood out as a fundamental challenge in the domain of renewable energy applications. The conventional boost converters face limitations in achieving the necessary high step-up conversion for renewable energy systems.
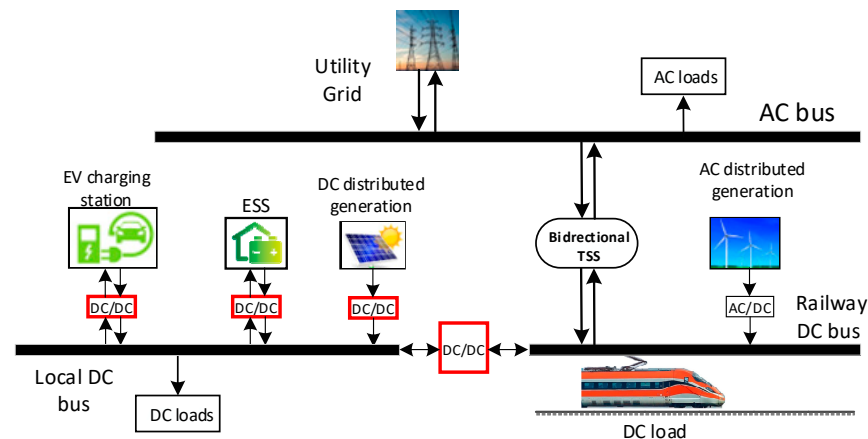
Figure 1. Schematic of a smart grid and microgrid with integrated DC–DC converters.

A comprehensive investigation into a family of two-level, isolated, bidirectional systems involving the use of DC–DC converters with pulse-width modulation and phase-shift (PPS) modulation has been documented [7]. Additionally, novel DC–DC converter topologies, including Cuk, SEPIC, and Zeta converters, based on critical conduction mode-operating capacitive link DC–DC converters, have been proposed [8]. These converters build upon quasi-square-wave zero-current converters, incorporating an auxiliary circuit for zero-current and zero-voltage switching, eliminating voltage ringing across the output switch [8].

A new control strategy for DC/DC buck converters is presented using artificial neural networks (ANNs) in [9]. The ANN, trained with approximation dynamic programming (ADP), enables proportional-integral (PI) control with error signals and their integrals. The DC/DC converter's voltage feedback to the ANN creates an equivalent system to a recurrent neural network, offering superior predictive control. Offline training is employed to prevent instability from weight changes in an online method.

In [10], minimal distortion point tracking (MDPT) is introduced for parallel-connected DC–DC converters, optimizing with phase-shifting switching waveforms. The control design enhances power quality, suggesting reduced reliance on passive filters.

For voltage step-down DC–DC converters with non-ideal components [11], an optimal transition approach is investigated, exhibiting robust performance even in the presence of parameter uncertainty. Ref. [12] demonstrates a non-isolated quadratic extended-duty-ratio

(EDR) boost converter, combining EDR and quadratic boost converters for high gain. The recommended Quadratic EDR (QEDR) boost converter achieves exceptional gain at low voltage and current stress, operating across diverse devices with moderate duty levels.

In [13], the authors explores PID controller design for buck converters, optimizing parameters using a particle swarm optimization (PSO) framework. An anti-windup control strategy is proposed, achieving effective voltage control despite input and load fluctuations. In [14], a time-based control DC/DC converter-specific integrated loop-gain-measuring circuit is proposed, minimizing its impact on regulator performance. Ref. [15] addresses balanced current sharing and voltage control in parallel-connected DC–DC converters, introducing a distributed dynamic control strategy resilient to variations.

Finally, [16–19] collectively present a design process utilizing a single quadratic Lyapunov function, Lyapunov–Metzler inequalities, and state feedback variable structure controllers for expedited convergence of DC–DC converters within a class of switched linear systems, as applied in [19] for the development of a sliding-mode controller according to the switched sliding.

Addressing the formidable challenge in stabilizing unstable systems through the definition of suitable switching rules is a focal point in the theory of switched systems. In efforts to mitigate the conservatism associated with stabilization methods for switched linear systems, [20–24] introduced efficient approaches. Ref. [20] specifically employed composite quadratic functions to stabilize autonomous linear-switched systems devoid of external input. By combining multiple quadratic functions to construct a Lyapunov function, this technique yielded sufficient conditions for formulating stabilizing switching laws in terms of bilinear matrix inequalities. Notably, superior outcomes were demonstrated when the number of quadratic functions surpassed the number of subsystems.

In response to the mentioned challenges, this paper introduces a rule for making switches in a way that ensures stability for linear-switched systems with constant external input. At the same time, it aims to minimize a guaranteed quadratic cost. A significant advancement here is the application of findings from [20] to switched affine systems with constant external input, specifically tailored to address the dynamic models of DC–DC converters. Unlike the other methods, the proposed control method in this paper is designed to minimize a certain cost. In contrast to the methods in [16,17], the proposed scheme introduces the idea of a composite switched Lyapunov function to create a control strategy for DC–DC converters. This new approach offers more flexibility in the design conditions, allowing for the selection of the number of quadratic terms in the Lyapunov function candidate.

Simulation results in Section 4 compare the performance of the proposed method against outcomes from [16], employing Buck and Buck–Boost circuits to illustrate the superior efficacy of the proposed method. Section 5 presents the experimental validation of the derived control scheme on the Buck converter, confirming its practical applicability. It is emphasized that the developed switching method can be extended to control various types of converters.

The paper is structured as follows. Section 2. delineates a switched system model for DC–DC converters and formulates the switching design problem. Section 3 introduces the necessary conditions for designing a switching strategy for the affine switched system. Comparative simulation results are presented in Section 4 to underscore the superiority of the proposed approach. Section 5 details the experimental results, showcasing the practical implementation of the designed switching method. The paper concludes in Section 6.

2. Methodology and Problem Statement

A DC–DC converter is defined as a switched system comprising multiple linear subsystems characterized by constant external inputs and sharing common state variables. Within this structure, the active subsystem, denoted as the one dictating the state evolution at any specific moment, stands out. The control parameters, determined by the switching rule, influence the activation of a particular subsystem. The dynamics of this converter can

be articulated through a state-space realization, encapsulating its behavior and interactions in a mathematical framework as

$$\dot{x}(t) = A_\sigma x(t) + B_\sigma u \tag{1}$$

In this context, the state vector, denoted as $x(t) \in \mathfrak{R}^n$, and the external input, represented as u, are assumed to be constant for all instances. The more explanation about the symbols can be found in Appendix A. The switching function, $\sigma(t) : t > 0 \rightarrow K \subset \aleph$, operates at each moment in time t, selecting a specific known subsystem from the available options. The primary goal is to formulate an optimal switching strategy, denoted as $\sigma(x(t))$, with the aim of minimizing the defined following performance index:

$$J_c = \int_0^\infty (x(t) - x_e)^T Q (x(t) - x_e) dt \tag{2}$$

In this formulation, $x_e \in X_e$ represents an attainable equilibrium point, and the matrices of each subsystem Q_i have compatible dimensions. Additionally, the set of all equilibrium points X_e is determined through the proposed switching strategy. The performance index J_c in Equation (2) penalizes the weighted deviation of each state variable from the desired equilibrium point. The inherent challenge in solving this control problem arises from the discontinuous nature of the switching function $\sigma(x(t))$. Consequently, instead of directly addressing this complexity, the focus is on minimizing the upper bound of the performance index J_c, characterized on the right-hand side of Equation (3):

$$\int_0^\infty (x(t) - x_e)^T Q (x(t) - x_e) dt < (x_0 - x_e)^T P (x_0 - x_e) \tag{3}$$

wherein symmetric positive definite matrix $P \in R^{n \times n}$ and x_0 denotes the initial state. It is worth noting that the right-hand side of (3) refers to the weighted Euclidean distance existing between the starting and final points.

In essence, the task in the control problem is to determine the switching function $\sigma(x(t))$. This function ensures the asymptotic stability of the equilibrium point x_e while satisfying the specified cost guarantee in Equation (3).

3. Design of Switching Controller

In this part, a method for designing switching signals for switched systems with constant input that is relevant to DC–DC converters is established using the idea of a composite Lyapunov function. The primary finding of the paper is stated in the subsequent theorem.

3.1. Theorem

Assume that the switched linear system (1) with fixed input $u(t) = u \in R^m$ is an external input, which is assumed to be constant for all t ≥ 0. Let $N \in \aleph$, $Q > 0$, and $x_e \in \mathfrak{R}^n$ be given. If there exist $\lambda \in \Lambda$ real scalars $\beta_{ij} > 0$ for $i \in K, j \in I[1, N]$ and equiponderant positive definite matrices $P_j \in R^{n \times n}$ for all $j \in I[1, N]$, such that

$$A_i^T P_j + P_j A_i + Q - \sum_{k=1}^N \beta_{jk} (P_j - P_k) < 0 \tag{4}$$

$$A_\lambda x_e + B_\lambda u = 0 \tag{5}$$

Then, the switching strategy can be calculated as

$$\sigma = \arg \min_{i \in K} \zeta' P (A_i x_e + B_i u) \tag{6}$$

with $\zeta = x - x_e$ and $P \leq P_j$ for $j \in I[1, N]$, which makes the equilibrium point x_e asymptotically stable and makes the guaranteed cost (3) hold.

3.2. Proof

A combined candidate function for Lyapunov V_{min} is constructed from the quadratic functions $V_j(\boldsymbol{\zeta}) = \boldsymbol{\zeta}^T P_j \boldsymbol{\zeta}$ as follows:

$$V min \{ V_j(\boldsymbol{\zeta}) : j \in I[1, N] \}_{min} \tag{7}$$

in which $P_j = P_j^T > 0, j \in I[1, N]$. Without losing the ability to generalize, it can be assumed that $VT_{r min}$, for all $r \in I[1, N_0]$. This truth can be expressed as $\boldsymbol{\zeta}^T (P_j - P_k) \boldsymbol{\zeta} \leq 0$, for all $j \in I[1, N_0]$ and $k \in I[1, N]$. The following matrix inequality is identical to the following inequality:

$$P_j - P_k \leq 0 \, j \in I[1, N_0], k \in I[1, N] \tag{8}$$

On the other hand, the rate of change over time for V_{min} in (7) along an arbitrary trajectory of the switched system (1) is calculated and forced to be negative by proper choice of switching strategy and its parameters. Note that

$$\dot{V} min \{ \dot{V}_j(\boldsymbol{\zeta}), j \in I[1, N_0] \}_{min} \tag{9}$$

wherein

$$\left\{ \begin{array}{l} \dot{V}_j(\boldsymbol{\zeta}) = \dot{\boldsymbol{x}}^T P_j \boldsymbol{\zeta} + \boldsymbol{\zeta}^T P_j \dot{\boldsymbol{x}} \\ = 2\boldsymbol{\zeta}^T P_j (A_\sigma \boldsymbol{x} + B_\sigma u) \end{array} \right\} \tag{10}$$

Substituting $\boldsymbol{x} = \boldsymbol{\zeta} + \boldsymbol{x}_e$ leads to

$$\dot{V}_j(\boldsymbol{\zeta}) = 2\boldsymbol{\zeta}^T P_j (A_\sigma \boldsymbol{x}_e + B_\sigma u) + \boldsymbol{\zeta}^T \left(A_\sigma^T P_j + P_j A_\sigma \right) \boldsymbol{\zeta} \tag{11}$$

Since $\sigma = \underset{i}{argmin} \boldsymbol{\zeta}^T P_j (A_i \boldsymbol{x}_e + B_i u)$, the following holds:

$$\left\{ \begin{array}{l} \dot{V}_j(\boldsymbol{\zeta}) = \underset{i \in K}{\min} \left[2\boldsymbol{\zeta}^T P_j (A_i \boldsymbol{x}_e + B_i u) \right] + \boldsymbol{\zeta}^T (A_\sigma^T P_j + P_j A_\sigma) \boldsymbol{\zeta} \\ \leq \underset{\lambda \in \Lambda}{\min} \left[2\boldsymbol{\zeta}^T P_j (A_\lambda \boldsymbol{x}_e + B_\lambda u) \right] + \boldsymbol{\zeta}^T (A_\sigma^T P_j + P_j A_\sigma) \boldsymbol{\zeta} \end{array} \right\} \tag{12}$$

Now, let us choose λ such that

$$\left\{ \begin{array}{l} A_\lambda \boldsymbol{x}_e + B_\lambda u = 0 \\ A_i^T P_j + P_j A_i < -Q \end{array} \right\} \tag{13}$$

or all $i \in K$; then, $\dot{V}_j(\boldsymbol{\zeta}) < -\boldsymbol{\zeta}^T Q \boldsymbol{\zeta}$, wherein Q is the weight matrix in (2). Regarding (9), the following is obtained:

$$\dot{V} T_{min} \tag{14}$$

Thus, the asymptotic stability of $\boldsymbol{x}_e$ is assured, as discussed in [20].

By S-procedure [25], the following can be the result of combining Inequalities (8) and (10):

$$A_i^T P_j + P_j A_i + Q - \sum_{k=1}^{N} \beta_{jk} (P_j - P_k) < 0 \tag{15}$$

where $\beta_{ij} \geq 0$ are real scalars. Furthermore, by integrating both sides of Equation (11) from $t = 0$ to $t = \infty$ while considering $P \leq P_j$ and regarding V_{min}, Relation (3) is obtained.

- Remark 1

The switching function σ in (6) relies on the matrix that is derived from solving the set of inequalities given by (4) and (5) that include bilinear terms (the product of scalar variables and matrix variables), as in [20]. In general, the path-following approach first presented in [26] can be used to efficiently solve the obtained BMIs.

- Remark 2

Because the modulation function in Equation (6) has a linear nature, it can be implemented in real-world scenarios.

Despite the fact that [16,17] offer a linear-switching law, the synthesis situations that must be managed are substantially more demanding than the design criterion that is presented in this study. In comparison to these studies, the proposed technique is less conservative. This claim will is examined using simulation results.

Regarding the potential of LMI-/BMI-based approaches, more practical requirements can be incorporated into the suggested theorem. For instance, inspired by [3], the extracted result is extended in the following corollary for the case that there exist bounds on the output peak.

3.3. Corollary

Contemplate the switched linear system in (1), given an initial condition $x(0)$ and constrained output $\|y(t)\| \leq y_{max}$, for $t \geq 0$. Let $N \in \aleph$, Q, $x_e \in \Re^n$, and $y_{\max} \in R$ be given. If there exist $\lambda \in \Lambda$ real scalars $\beta_{ij} > 0$ for $i \in K$, $j \in I[1, N]$ and symmetric positive decisive matrices $P_j \in R^{n \times n}$ for all $j \in I[1, N]$, as:

$$
\left\{
\begin{array}{l}
\left[\begin{array}{c} P_j C^T \\ C y_{max}^2 \end{array} \right] \\[2em]
\left[\begin{array}{c} I\zeta^T(0)P_j \\ P_j \zeta(0) P_j \end{array} \right] > 0 \\[1em]
A_i^T P_j + P_j A_i + Q - \sum_{k=1}^{N} \beta_{jk}(P_j - P_k) < 0 \\[0.5em]
A_\lambda x_e + B_\lambda u = 0
\end{array}
\right\}
\tag{16}
$$

wherein $\zeta = x - x_e$ and I is identity matrix, then the switching strategy in (6), with $P \leq P_j$ for all $j \in I[1, N]$, makes the equilibrium point x_e globally asymptotically stable and the guaranteed cost in (3) holds.

4. Simulations Results and Comparison

To demonstrate the suggested controller's superior performance versus the competing one in [16], the Buck and Buck–Boost converters were simulated while applying the design-switching strategy in the Simulink package in MATLAB®2022a.

In Figure 2, schematic diagrams of the Buck and Buck–Boost converters feeding a resistive load are recalled from [16], where i_L and v_c, respectively, stand for the inductor current and the capacitor voltage. In Figure 2, S_1 is the power electronic switch and S_2 is the diode, where C_0 is the stabilizing capacitor, which decreases the voltage fluctuation across the load and lets the ripple current pass through, hence maintaining the constant current flow across the load.

(**a**)   (**b**)
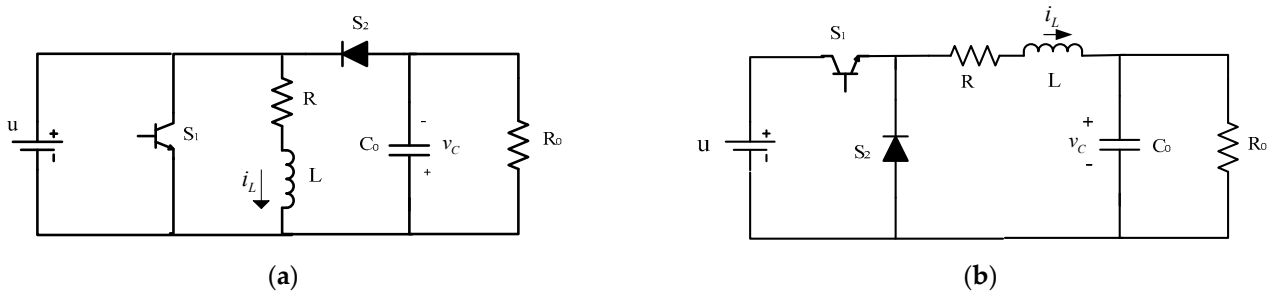
Figure 2. Schematic diagram of (**a**) the Buck–Boost and (**b**) the Buck converters.

The Buck–Boost converter in Figure 2a is modeled as a switched system in the form of (1) that consists of two affine subsystems with state vector $x(t) = \begin{bmatrix} i_L(t) & V_c(t) \end{bmatrix}^T$ and the following matrices:

$$\left\{ \begin{array}{l} A_1 = \begin{bmatrix} -\frac{R}{L} & 0 \\ 0 & -\frac{1}{R_o C_o} \end{bmatrix}, B_1 = \begin{bmatrix} \frac{1}{L} \\ 0 \end{bmatrix} \\[4mm] A_2 = \begin{bmatrix} -R/L & -1/L \\ 1/C_0 & -1/R_0 C_0 \end{bmatrix}, B_2 = \begin{bmatrix} 0 \\ 0 \end{bmatrix} \end{array} \right\} \tag{17}$$

The total number of equilibrium points that can exist is determined as

$$X_e = \left\{ (i_e, v_e) : 0 \leq v_e \leq R_0 i_e, v_e^2 + (RR_0) i_e^2 - (R_0 u) i_e + u v_e = 0 \right\} \tag{18}$$

The achieved voltage range is approximated as $0 \leq v_e \leq \left(\sqrt{\frac{R_0}{4R}} \right) u$; whenever the load resistance and source impedance align, $R << R_0$.

The Buck converter in Figure 1b is described in the form of (1) with two subsystems with the state vector $x(t) = \begin{bmatrix} i_L(t) v_c(t) \end{bmatrix}^T$ and the following matrices:

$$\left\{ \begin{array}{l} A_1 = A_2 = \begin{bmatrix} -\frac{R}{L} & \frac{-1}{L} \\ \frac{1}{C_0} & -\frac{1}{R_0 C_0} \end{bmatrix} \\[4mm] B_1 = \begin{bmatrix} \frac{1}{L} \\ 0 \end{bmatrix}, B_2 = \begin{bmatrix} 0 \\ 0 \end{bmatrix} \end{array} \right\} \tag{19}$$

The following formula is used to calculate the set of all possible equilibrium points in the Buck–Boost circuit:

$$X_e = \{ (i_e, v_e) : v_e = R_0 i_e, 0 \leq i_e \leq u / (R_0 + R) \} \tag{20}$$

given that the resistance of the load and the source satisfy $R << R_0$.

The performance index in (2) is rewritten as follows for the considered circuits:

$$J_c = \int_0^\infty R_0^{-1} [v_c(t) - v_e]^2 + \rho R [i_L(t) - i_e]^2 dt \tag{21}$$

The values of the elements of circuits are taken from [16] as $u = 100$ V, $R = 2$ Ω, $L = 500$ μH, $C_0 = 470$ μF, and $R_0 = 50$ Ω. Similar to [16], the weight matrix parameter ρ in (13) is selected to be zero, which is equivalent to the following cost weight:

$$Q = \begin{bmatrix} 0 & 0 \\ 0 & \frac{1}{R_0} \end{bmatrix} \tag{22}$$

The matrix inequalities in the Theorem are solved by YALMIP to obtain the parameters of the switching strategy in (6), which are applied to each circuit in the simulation scenarios.

Time responses of the states in the Buck–Boost converter are shown in Figure 3 for $v_e = 20$ V. As seen, the transient behavior of the suggested converter is noticeably faster than the one developed in [16]. More specifically, settling times of the outputs in the proposed converter and the rival one in [16] equal, respectively, 8.5 and 9 ms.

(a)

(b)
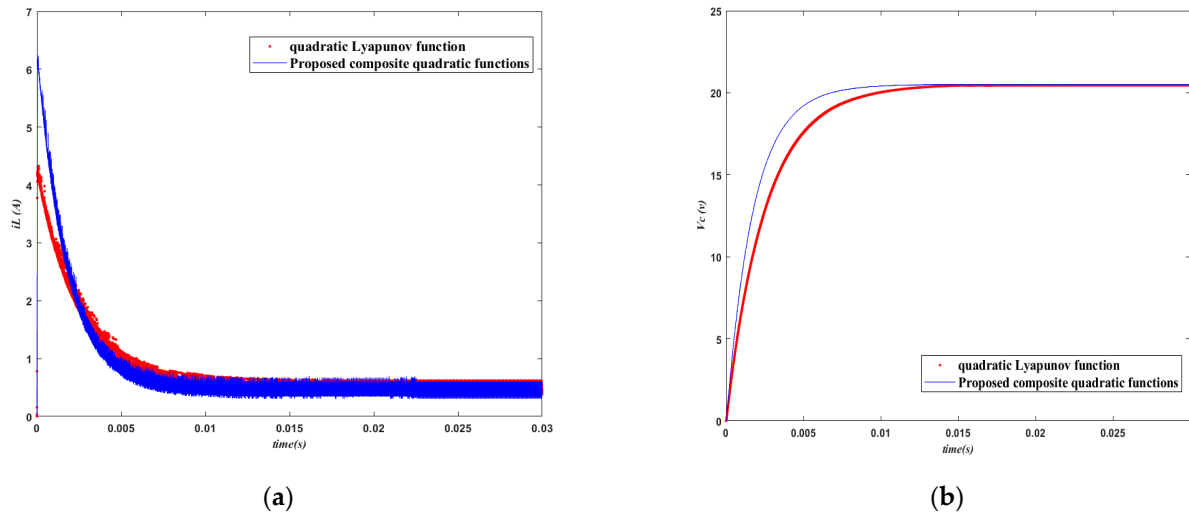
Figure 3. Trajectories of (**a**) the inductor current and (**b**) the output voltage in the Buck–Boost.

To compare the proposed design method with the one in [16], the performance index J_c in (13) was extracted. A summary is presented in Table 1 for five distinct desired working points. The converter results obtained using the suggested control strategy are improved by up to 30% compared to the results achieved by the scheme in [16], which confirms the effectiveness of the proposed method.

Table 1. Comparison of the performance index for various equilibrium points in the Buck–Boost converter.

Performance Index J_c		Desired Equilibrium Point
[12]	**Proposed Method**	
0.0779	0.0599	$v_e = 50$
0.0457	0.0346	$v_e = 40$
0.0236	0.0173	$v_e = 30$
0.0099	0.0071	$v_e = 20$
0.0023	0.0016	$v_e = 10$

Figure 4 depicts the time response of the states of the Buck converter for $v_e = 20$ V. As can be seen, the transient response of the suggested converter is faster than the one proposed in [16].

(a)

(b)
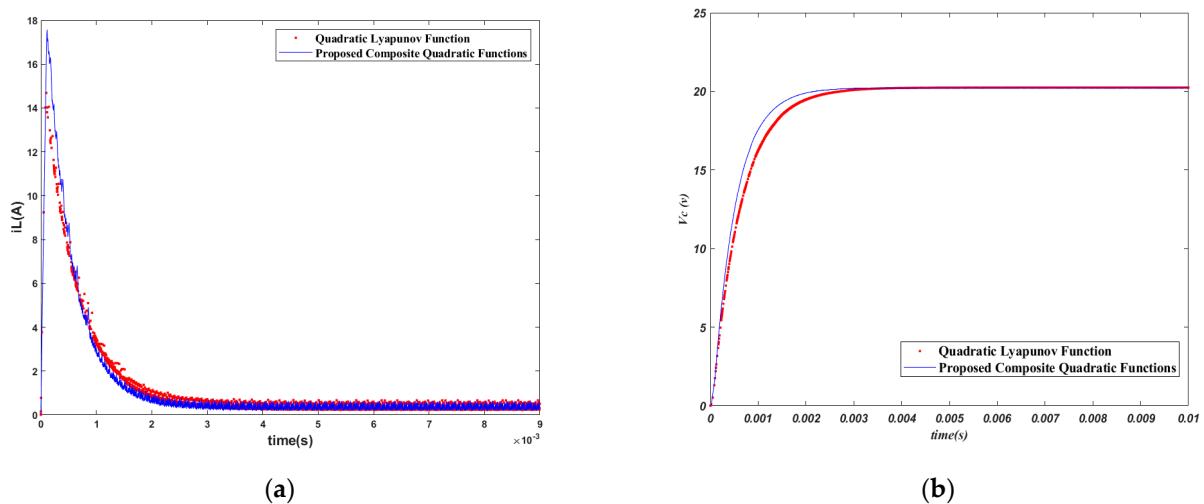
Figure 4. Waveforms of (**a**) the inductor current and (**b**) the output voltage in the Buck.

The performance index J_c for the Buck circuit is mentioned in Table 2 for five desired equilibrium points. The result obtained using the specified controller is improved up to about 20% with respect to the results obtained by the mentioned rival method.

Table 2. Comparison of the performance index for different output voltages in Buck.

Performance Index J_c		Desired Equilibrium Point
[12]	**Proposed Method**	
0.0126	0.0111	$v_e = 40$
0.0067	0.0056	$v_e = 30$
0.0028	0.0022	$v_e = 20$
0.00065	0.00051	$v_e = 10$

Moreover, Figures 5 and 6 illustrate the resilience of the Buck circuit's output voltage against periodic step changes in the load resistor and source voltage, respectively. In the first simulation scenario, the load resistor is altered instantly from its nominal value of 2 Ω to 10 Ω and vice versa periodically. In the next simulation setup, the input voltage was varied suddenly from its nominal value of 100 V to 70 V and vice versa, intermittently. It is evident that satisfactory output regulation is achieved by the proposed method in the presence of load and source disturbances.

(**a**)

(**b**)
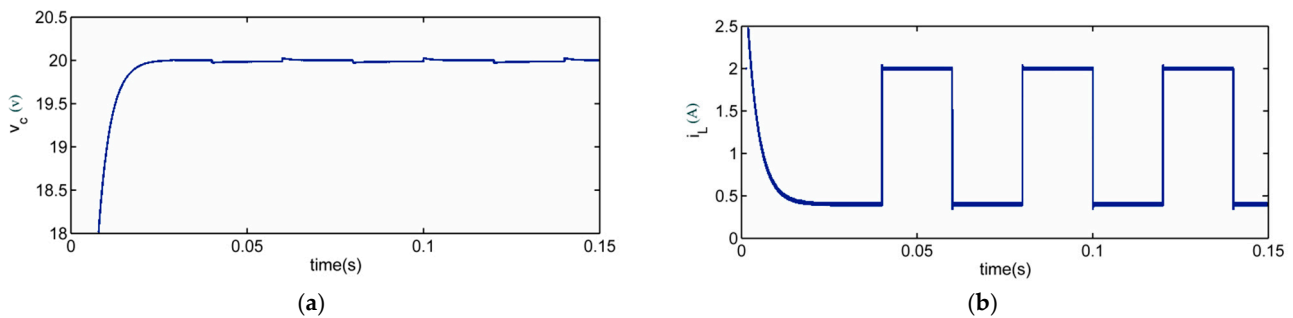
Figure 5. The observed time response of the Buck converter's to periodic step changes in the resistor value. (**a**) Output voltage (**b**) Inductor current.

(**a**)

(**b**)
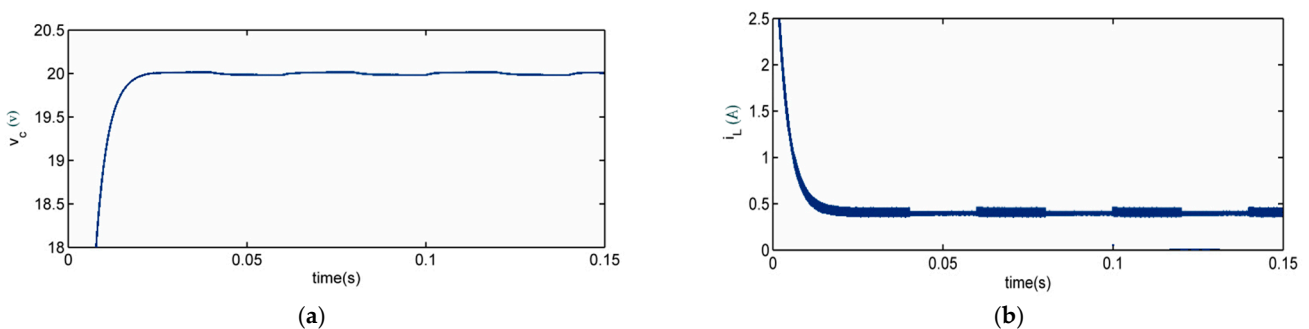
Figure 6. The change in output voltage and inductor current of the Buck converter in response to cyclic variations in the input voltage, observed over a period of time. (**a**) Output voltage (**b**) Inductor current.

Furthermore, to evaluate the performance of the proposed method in the presence of both load and source interference, changes in both load and source were made (u = 120, $R_0 = 20$). The output results are shown in Figure 7, and we can confirm that the proposed method is sufficiently robust to the interferences.

(**a**)

(**b**)
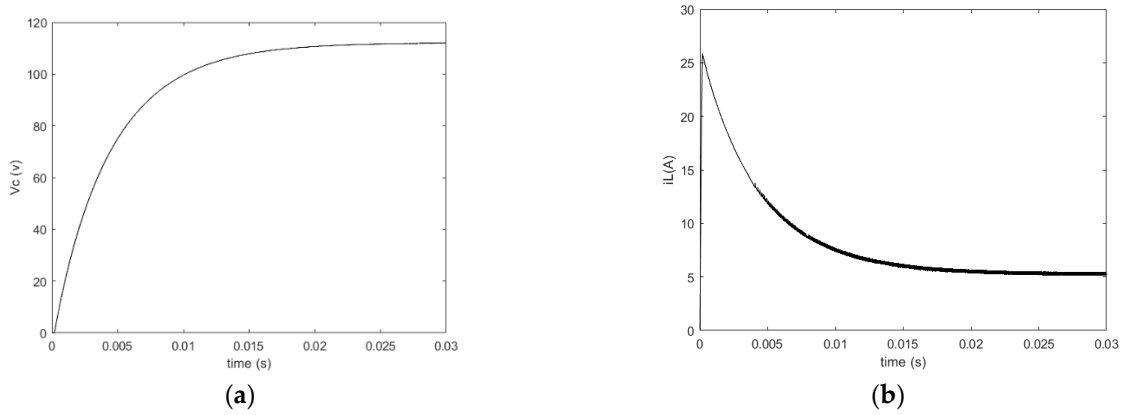
Figure 7. The change in output voltage and inductor current of the Buck converter in response to cyclic variations in the input voltage, observed over a period of time: (**a**) output voltage, (**b**) inductor current.

To confirm the performance of the method in different working situations, the input voltage was also considered as $V_e = 50$ and $V_e = 10$. The results are shown in Figure 8.

(**a**)

(**b**)

(**c**)

(**d**)
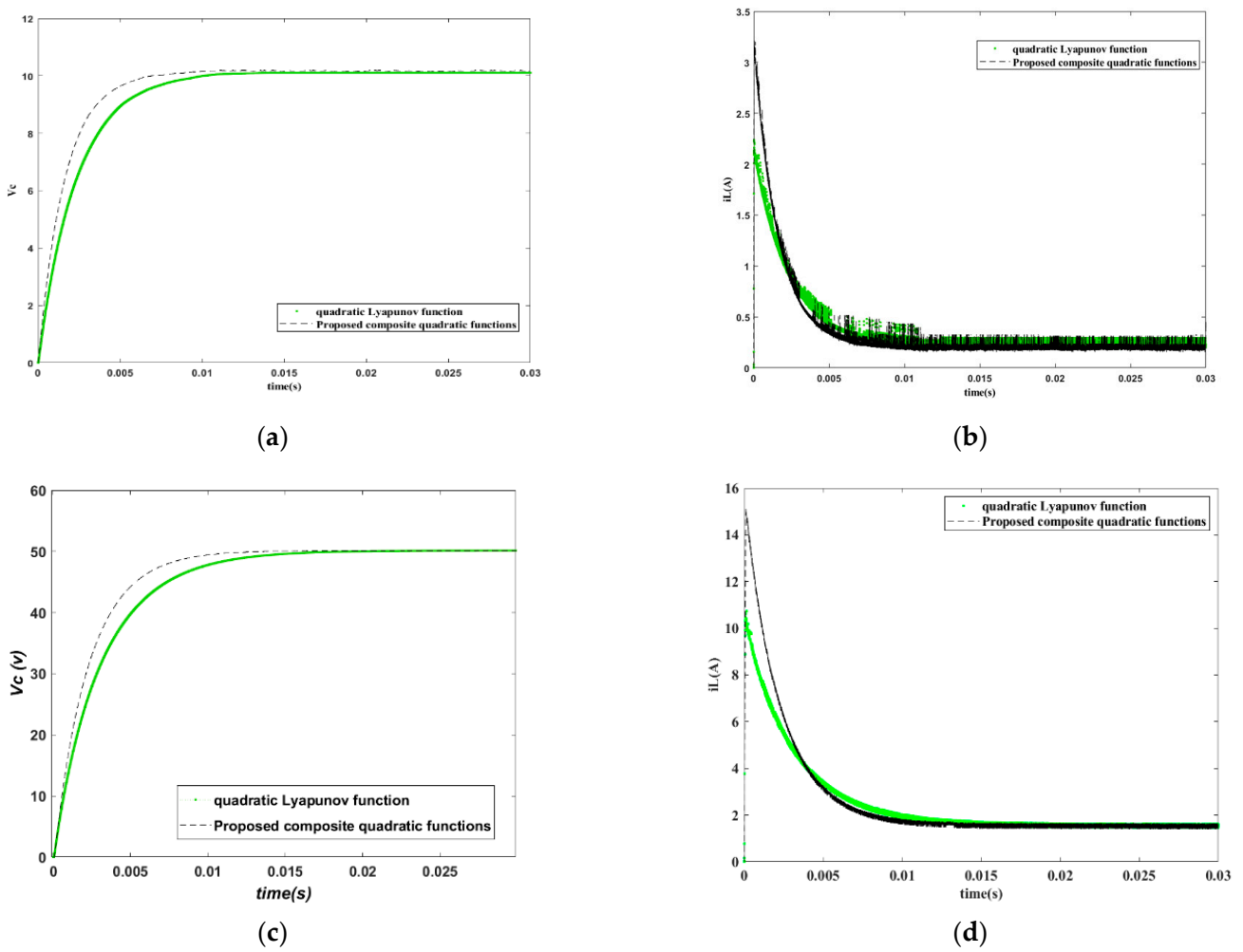
Figure 8. Change in the output voltage and inductor current of the Buck converter in response to cyclic variations in the input voltage, observed over a period of time: (**a**) output voltage with $V_e = 10$ V (**b**) inductor current with $V_e = 10$ V (**c**) output voltage with $V_e = 50$ V (**d**) inductor current with $V_e = 10$ V.

5. Experimental Results

In order to verify the practical applicability of the proposed method, the Buck converter was realized with the general structure shown in Figure 9a. The converter was composed of a power MOSFET module that provided the converter leg. A gate driver was employed to amplify the control signal for application to the MOSFET gates. The converter component values were the same as the simulation circuit in the preceding section, except u, which was set to be 35 V to adapt to our laboratory hardware limitations. The experimental prototype developed in the lab is shown in Figure 9b.
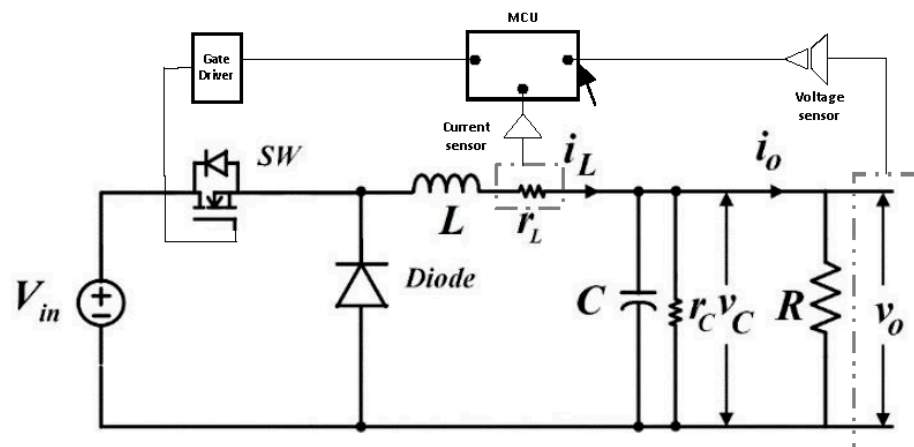
(a)
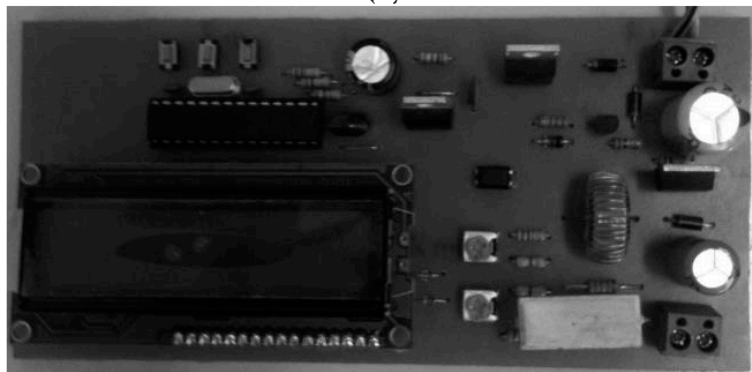
(b)

Figure 9. Schematic diagram of Buck converter (**a**) and developed experimental prototype of Buck converter (**b**).

The proposed control relation in (6), implemented through the use of an 8-bit AVR microcontroller operating at an external clock frequency of 16 MHz, utilized a shunt resistance and a differential voltage measurement circuit to gauge the inductor current. Analog-to-digital conversion was performed with 10-bit resolution to acquire and convert the output voltage and coil current. The analog-to-digital sampling process took 37 μs.

Waveforms were captured utilizing a digital oscilloscope. Figure 10 displays the measured response of the converter capacitor (output) voltage and inductor current waveforms, along with the corresponding simulation results.

The concordance between the experimental findings and numerical simulations is evident, as evidenced by the congruent transient and steady-state behaviors observed in both the simulation and experimental output voltages. Figure 11 displays the Fast Fourier Transform (FFT) of the output voltage, providing further insights into its frequency components. In Figure 12, the converter output voltage is depicted alongside the MOSFET switching waveform, shedding light on the interplay between these crucial signals. Zooming in on the steady state of the output voltage waveform and the switching signal,

Figure 13 provides a detailed examination of their characteristics. Moreover, Figure 14 presents the control signal and its FFT during the steady state, showcasing how the fluctuation of current has been successfully reduced. This comprehensive analysis not only underscores the agreement between experimental and simulated results, but also highlights the efficacy of the control strategy in mitigating current fluctuations, as corroborated by the frequency-domain analysis using FFT.

(**a**)

(**b**)
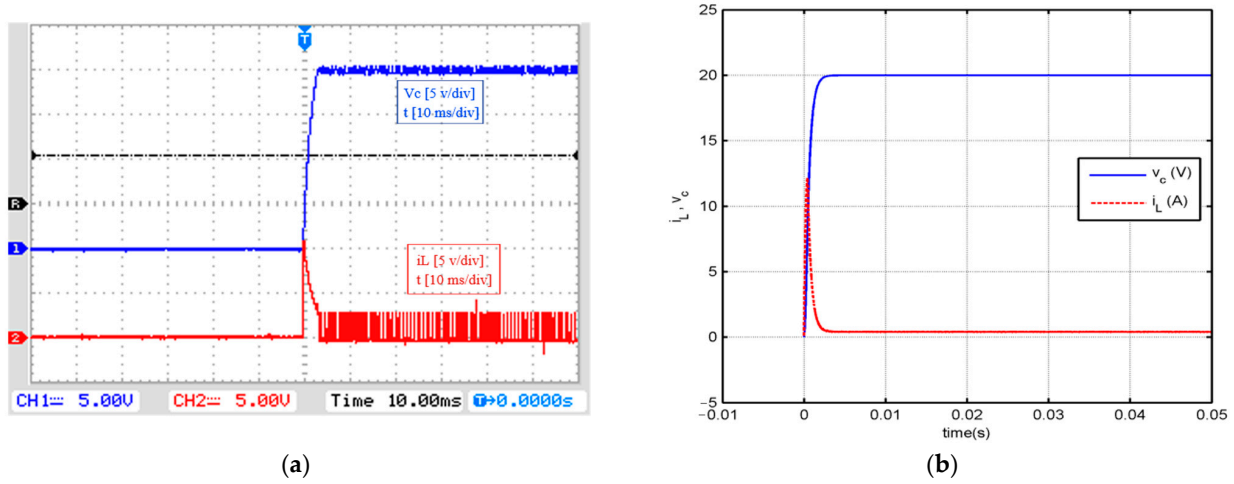
Figure 10. Output voltage and inductor current for $u = 35$ V: (**a**) Experiment (**b**) Simulation.
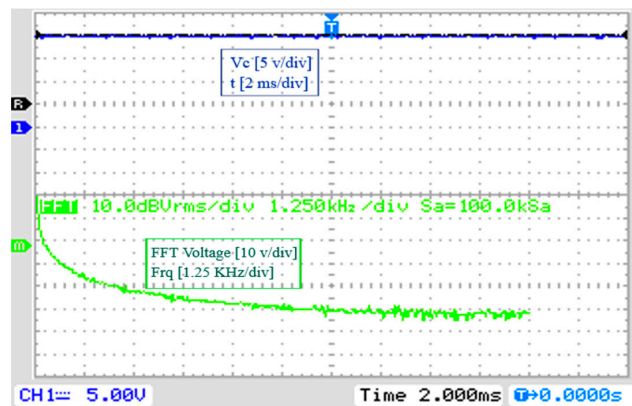
Figure 11. Experimental result of the output voltage's FFT.
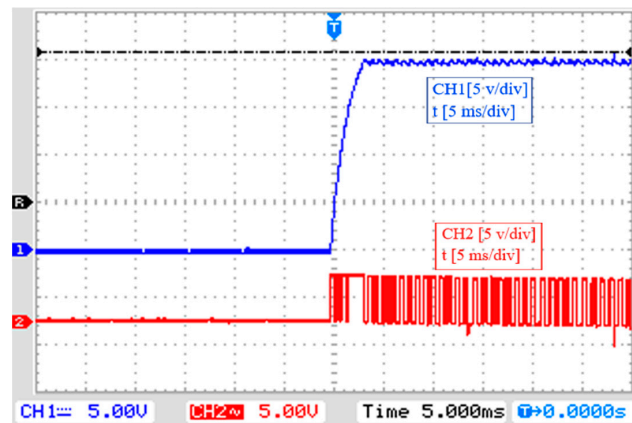
Figure 12. Experimental results of the output voltage and the switching signal (CH1: Output Voltage, CH2: Switching Pulses).
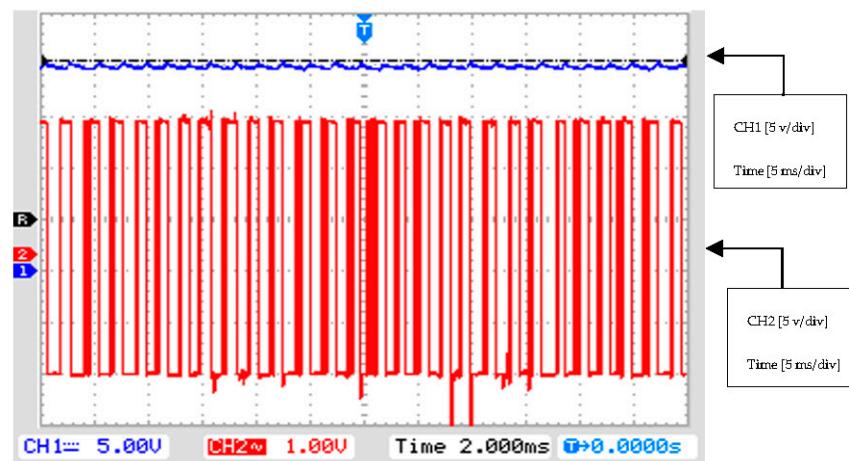
Figure 13. A closer look at the output voltage and switching waveforms in steady state (CH1: Output Voltage, CH2: Switching Pulses).
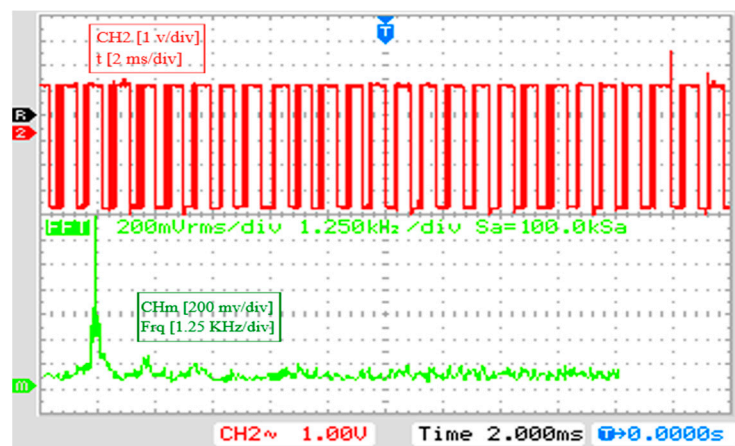
Figure 14. Experimental results of the steady-state switching signal and its FFT (CH2: Switching Signal, CHm: Output Voltage).

6. Conclusions

In conclusion, this paper has successfully expanded upon an efficient technique for deriving a stabilizing state-feedback switching law, originally designed for autonomous switched systems, to encompass affine switched systems with constant external input. The novel switching strategy introduced in this paper not only ensures stability but also minimizes a quadratic guaranteed cost, demonstrating its versatility and applicability to a broader class of systems. The efficacy of the proposed design approach was substantiated through simulations on classical Buck and Buck–Boost converters, illustrating the simplicity and effectiveness of the strategy.

A crucial aspect of this research involves a comparative analysis with a recent approach, revealing that the proposed method enhances the design performance criterion by approximately 30% when compared to the competing strategy. This significant improvement underscores the practical viability and superiority of the introduced approach, making it a compelling choice for control subsystems in advanced converter circuits.

The experimental validation using a Buck circuit further underscores the real-world applicability of the proposed method, demonstrating its robustness and reliability in practical settings. Importantly, the proposed Lyapunov-based method stands out for its remarkable robustness, speed, and accuracy, providing a notable advantage over alternative approaches.

Looking ahead, the applications of this method extend beyond theoretical advancements. The proposed approach holds great promise for addressing the challenges posed by renewable energy sources. By leveraging composite-switched Lyapunov functions, the method is poised to play a pivotal role in optimizing power transfer, improving stability, and ensuring reliable operation in diverse RES environments. This is particularly relevant as RES integration becomes increasingly integral to the pursuit of sustainable and eco-friendly power solutions. The proposed method not only offers a robust solution for addressing the inherent challenges of renewable energy systems but also paves the way for enhancing the overall efficiency and performance of RES integration in power systems.

Author Contributions: In the process of preparing this manuscript, T.H. and R.M.E. were responsible for executing the methodology, managing data curation, conducting software-based simulations, obtaining experimental results, and drafting the original written content. On the other hand, H.J.K. undertook the tasks of editing, validation, visualization, handling resources, and funding acquisition, as well as contributing to editing and supervision. All authors have read and agreed to the published version of the manuscript.

Appendix A

$\Re$ represents the set of real numbers, and $\aleph$ represents the set of natural numbers. $I[k_1, k_2]$ symbolizes the set containing all integers within the range from k_1 to k_2. The notation $M > 0$ ($M \geq 0$) signifies that M is a real-symmetric positively definite (or positive semi-definite) matrix. The superscript T denotes matrix transposition. Λ denotes the set of all non-negative vectors. $\lambda = \left[\lambda_1 \lambda_2 \cdots \lambda_N\right]^T$ with the property $\sum_{i=1}^{N} \lambda_i = 1$. The convex combination of matrices $\{A_1, \cdots, A_N\}$ is defined as $A_\lambda = \sum_{i=1}^{N} \lambda_i A_i$.

References

1. Hasanpour, S.; Siwakoti, Y.P.; Blaabjerg, F. A New High Efficiency High Step-Up DC/DC Converter for Renewable Energy Applications. *IEEE Trans. Ind. Appl.* **2022**, *70*, 1489–1500. [CrossRef]
2. Forouzesh, M.; Siwakoti, Y.P.; Gorji, S.A.; Blaabjerg, F.; Lehman, B. Step-up DC–DC converters: A comprehensive review of voltage-boosting techniques, topologies, and applications. *IEEE Trans. Power Electron.* **2017**, *32*, 9143–9178. [CrossRef]
3. Chakraborty, S.; Vu, H.-N.; Hasan, M.M.; Tran, D.-D.; Baghdadi, M.E.; Hegazy, O. DC-DC Converter Topologies for Electric Vehicles, Plug-in Hybrid Electric Vehicles and Fast Charging Stations: State of the Art and Future Trends. *Energies* **2019**, *12*, 1569. [CrossRef]
4. Kaleybar, H.J.; Brenna, M.; Foiadelli, F.; Zaninelli, D. Electric Railway System Integrated with EV Charging Station Realizing Train-to-Vehicle Technology. *IEEE Trans. Veh. Technol.* **2023**. [CrossRef]
5. Kaleybar, H.J.; Brenna, M.; Castelli-Dezza, F.; Zaninelli, D. Sustainable MVDC Railway System Integrated with Renewable Energy Sources and EV Charging Station. In Proceedings of the 2022 IEEE Vehicle Power and Propulsion Conference (VPPC), Merced, CA, USA, 1–4 November 2022; pp. 1–6. [CrossRef]
6. Ahmadi, M.; Jafari Kaleybar, H.; Brenna, M.; Castelli-Dezza, F.; Carmeli, M.S. Integration of Distributed Energy Resources and EV Fast-Charging Infrastructure in High-Speed Railway Systems. *Electronics* **2021**, *10*, 2555. [CrossRef]
7. Li, S.; Xiangli, K.; Smedley, K.M. Analysis and design of a family of two-level PWM plus phase-shift-modulated DC–DC converters. *IEEE Trans. Ind. Electron.* **2017**, *65*, 4650–4660. [CrossRef]
8. Khodabandeh, M.; Afshari, E.; Amirabadi, M. A family of Ćuk, Zeta, and SEPIC based soft-switching DC–DC converters. *IEEE Trans. Power Electron.* **2019**, *34*, 9503–9519. [CrossRef]
9. Dong, W.; Li, S.; Fu, X.; Li, Z.; Fairbank, M.; Gao, Y. Control of a buck DC/DC converter using approximate dynamic programming and artificial neural networks. *IEEE Trans. Circuits Syst. I Regul. Pap.* **2021**, *68*, 1760–1768. [CrossRef]

10. Poon, J.; Johnson, B.B.; Dhople, S.V.; Sanders, S.R. Minimum distortion point tracking: Optimal phase shifting for input-or output-parallel connected dc-dc converters. In Proceedings of the 2018 IEEE 19th Workshop on Control and Modeling for Power Electronics (COMPEL), Padova, Italy, 25–28 June 2018; Volume 25, pp. 1–6.

11. Heydari, A. Optimal switching of DC–DC power converters using approximate dynamic programming. *IEEE Trans. Neural Netw. Learn. Syst.* **2016**, *29*, 586–596. [CrossRef] [PubMed]

12. Gupta, A.; Korada, N.; Ayyanar, R. Quadratic-Extended-Duty-Ratio Boost Converters for Ultra High Gain Application with Low Input Current Ripple and Low Device Stress. *IEEE Trans. Ind. Appl.* **2022**, *59*, 938–948. [CrossRef]

13. Debnath, A.; Olowu, T.O.; Roy, S.; Parvez, I.; Sarwat, A. Particle Swarm Optimization-based PID Controller Design for DC-DC Buck Converter. In Proceedings of the 2021 North American Power Symposium (NAPS), College Station, TX, USA, 14 November 2021.

14. Leoncini, M.; Melillo, P.; Bertolini, A.; Levantino, S.; Ghioni, M. Integrated Loop-Gain Measurement Circuit for DC/DC Boost Converters with Time-Based Control. In Proceedings of the 2022 17th Conference on Ph.D. Research in Microelectronics and Electronics (PRIME), Villasimius, Italy, 12 June 2022.

15. Sadabadi, M.S. A distributed control strategy for parallel DC-DC converters. *IEEE Control Syst. Lett.* **2020**, *5*, 1231–1236. [CrossRef]

16. Deaecto, G.S.; Geromel, J.C.; Garcia, F.S.; Pomilio, J.A. Switched affine systems control design with application to DC-DC converters. *IET Control Theory Appl.* **2010**, *4*, 1201–1210. [CrossRef]

17. Júnior, E.M.; Teixeira, M.C.M.; Cardim, R.; Moreira, M.R.; Assunção, E.; Yoshimura, V.L. On control design of switched affine systems with application to DC-DC converters. In *Frontiers in Advanced Control Systems*; de Oliveira Serra, G.L., Ed.; Intech: London, UK, 2012.

18. Cardim, R.; Teixeira, M.C.; Assuncao, E.; Covacic, M.R. Variable-structure control design of switched systems with an application to a DC-DC power converter. *IEEE Trans. Indestrial Electron.* **2009**, *56*, 3505–3513. [CrossRef]

19. Noori, A.; Farsi, M.; Mahboobi Esfanjani, R. Design and implementation of a robust switching strategy for DC–DC converters. *IET Power Electron.* **2016**, *9*, 316–322. [CrossRef]

20. Hu, T.; Ma, L.; Lin, Z. Stabilization of Switched Systems via Composite Quadratic Functions. *IEEE Trans. Autom. Control* **2008**, *53*, 2571–2585. [CrossRef]

21. Hashemi, T.; Farnam, A.; Esfanjani, R.M.; Kojabadi, H.M. A new approach to design switching strategy for the buck converters. In Proceedings of the 4th Annual International Power Electronics, Drive Systems and Technologies Conference, Tehran, Iran, 13–14 February 2013.

22. Soldado-Guaman, J.; Herrera-Perez, V.; Pacheco-Cunduri, M.; Paredes-Camacho, A.; Delgado-Prieto, M.; Henandez-Ambato, J. Multiple Input-Single Output DC-DC Converters Assessment for Low Power Renewable Sources Integration. *Energies* **2023**, *16*, 1652. [CrossRef]

23. Du, R.; Samavatian, V.; Samavatian, M.; Gono, T.; Jasiński, M. Development of a High-Gain Step-Up DC/DC Power Converter with Magnetic Coupling for Low-Voltage Renewable Energy. *IEEE Access* **2023**, *11*, 90038–90051. [CrossRef]

24. Baba, M.F.; Giridhar, A.V.; Narasimharaju, B.L. A Wide Voltage Range Bidirectional High Voltage Transfer Ratio Quadratic Boost DC-DC converter for EVs with Hybrid Energy Sources. *IEEE J. Emerg. Sel. Top. Ind. Electron.* **2023**, 1–10. [CrossRef]

25. Boyd, L.; Feron, E.; Balakrishnan, V. *Linear Matrix Inequalities in Systems and Control Theory*; SIAM: Philadelphia, PA, USA, 1994; pp. 157–193.

26. Hassibi, A.; How, J.; Boyd, S. A path-following method for solving BMI problems in control. In Proceedings of the American Control Conference, San Diego, CA, USA, 2 June 1999.